ELSEVIER

Journal of Nuclear Materials 250 (1997) 176–183

journal of nuclear materials

Influence of long-term thermal aging on the microstructural evolution of nuclear reactor pressure vessel materials: an atom probe study

P. Pareige [1], K.F. Russell, R.E. Stoller, M.K. Miller *

Metals and Ceramics Division, Oak Ridge National Laboratory, PO Box 2008, Oak Ridge, TN 37831-6376, USA

Received 5 February 1997; accepted 28 July 1997

Abstract

Atom probe field ion microscopy (APFIM) investigations of the microstructure of unaged (as-fabricated) and long-term thermally-aged (~ 100 000 h at 280°C) surveillance materials from commercial reactor pressure vessel steels were performed. This combination of materials and conditions permitted the investigation of potential thermal aging effects. This microstructural study focused on the quantification of the compositions of the matrix and carbides. The APFIM results indicate that there was no significant microstructural evolution after a long-term thermal exposure in weld, plate and forging materials. The matrix depletion of copper that was observed in weld materials was consistent with the copper concentration in the matrix after the stress relief heat treatment. The composition of cementite carbides aged for 100 000 h were compared to the Thermocalc™ prediction. The APFIM comparisons of materials under these conditions are consistent with the measured change in mechanical properties such as the Charpy transition temperature. © 1997 Elsevier Science B.V.

1. Introduction

Surveillance programs for nuclear reactor vessels were primarily designed to monitor the radiation-induced changes occurring in the mechanical properties of the pressure vessel materials. Nowadays, a large set of data is available on the mechanical properties and also the microstructural evolution of irradiated materials. The embrittlement of vessel steels and weldments is known to be related to the presence of residual elements such as copper and phosphorus. Recent microstructural investigations have conclusively shown that the presence of these elements leads to the radiation-enhanced or radiation-induced formation of ultrafine copper-enriched clusters associated with nickel, manganese, silicon, phosphorous and iron and phosphorous clusters in high phosphorous materials [1–12]. However, this evolution of the microstructure has been observed in materials that have been neutron-irradiated for several years at temperatures near 290°C. It is therefore possible that some of the degradation in mechanical properties may be a result of the long-term thermal aging component.

Some previous research has indicated the potential for thermal degradation of the mechanical properties of materials used in the construction of nuclear power systems when they are operated at relatively high temperatures (> 371°C) [13]. However, degradation in properties as a result of long-term exposure at lower temperatures (~ 300°C) is still an open question [14].

Among the studies on pressure vessel steels, Pense et al. [15] detected no shift in the ductile-to-brittle transition temperature (DBTT) of an A302 Mn–Mo plate steel after a relatively short aging time of 500 h at 370°C. After the same aging time, an A203 Mn–Ni steel exhibited shifts in the transition temperature in excess of 40°C. Thermal aging data are also available for a SA-302B steel for periods of 9,726 h and 26,114 h at 307°C; these data were reported from the surveillance program of the Big Rock

* Corresponding author. Fax: +1-423 574 7659.

[1] Present address: Laboratoire de Microscopie Ionique et Electronique, GMP-UMR 6634, Faculté des Sciences de l'Université de Rouen, 76128 Mont Saint Aignan cedex, France. Tel.: +33-2 35 14 68 78; fax: +33-2 35 14 66 52; e-mail: philippe.pareige@univ-rouen.fr.

PII S0022-3115(97)00264-X

Point Reactor (BRP) [16,17]. These data indicated little effect of thermal aging on the Charpy impact results of both the SA-302, grade B modified steel (which is equivalent to the current SA-533, grade B1 steel) base metal and weld metal. Also, one capsule from the Oconee Unit 1 PWR aged at 304°C for 15,800 h showed no significant shift in DBTT for the same materials as described above [18]. Recent results [19] concerning materials removed from Oconee Unit 3, aged for 103,000 h at 280°C, and from Arkansas Unit 1, aged for 93 000 h at 280°C, have shown that thermal aging had only a minor effect on the impact properties of both SA-302B base and weld metal. Changes resulting from thermal aging were of such small magnitude as to be considered insignificant. It was concluded [19] that ''If low temperature thermal ageing affects the fracture toughness of the materials, such changes cannot be monitored by the Charpy V-notch test. To further investigate the thermal ageing behavior on the fracture properties of reactor vessel steels, additional evaluations on the aged materials will include tension testing, fracture toughness and *microstructural investigations*.''

The main objective of the work presented in this paper was to use the technique of atom probe field ion microscopy to characterize the microstructure and the composition of low temperature (~ 300°C) long-term ($\sim 100\,000$ h) thermally-aged plate, forging and weld materials from the B&W Master Integrated Reactor Vessel Surveillance Program in order to investigate the potential thermal aging effects. It is important to determine if there are any changes in the composition of the matrix and if any ultra-fine precipitates had formed due to the thermal component of the service environment only. These investigations focussed on the copper and phosphorous as they are related to the embrittlement of pressure vessel steels and weldments during neutron irradiation. If such changes are observed, they would provide an early indication of the potential for thermal embrittlements at the longer ($\sim 300\,000$ h) times associated with the vessel lifetime. In addition, unaged specimens were investigated with the atom probe in order to establish a baseline so that the effects of long term exposure to temperature alone could be evaluated.

2. Materials description

Five structural steels were selected for the examination of long-term thermal aging effects. Both Oconee Unit 3 and Arkansas Unit 1 reactors have thermal aging boxes containing pieces of surveillance materials. The material removed from the thermal aging boxes included forging, plate and two weld metals. The base and weld metals are representative of the materials used to fabricate the beltline shell course regions of the Oconee Unit 3 and Arkansas Unit 1 reactor pressure vessels. In addition, the boxes contained ASTM correlation monitor plate material. The base metal materials were SA-533, grade B, class 1 plate steel and SA-508, class 2 forging steel. The two weld metals were typical Mn–Mo–Ni weld wire, Linde 80 flux submerged arc welds. The chemical compositions of the five materials are reported in Table 1.

The specimen aging capsules were located in one of the holder tubes used for irradiation on the service structure support of the reactor vessel heads. The boxes were located under the head insulation to help maintain the aging temperature. It was within the flow of the entering coolant which helped maintain the capsule at the same temperature as the reactor vessel wall. As a result of the location of these boxes, the surveillance material was exposed to an actual neutron fluence of less than 1×10^{14} n m^{-2} (i.e., less than 1.5×10^{-11} dpa) or essentially zero insofar as material damage is concerned. The exact exposure time for each set of materials was difficult to determine because of the time allowance for reactor heat up, cool down and hot standby. The aging times given in Table 2 for these materials reflect a 10% increase of the actual effective full

Table 1
Chemical composition (bulk chemistry) of B&W Owners Group surveillance materials, balance iron

Identification	%	Cu	Ni	Mn	Si	P	C	S	Mo	Cr
Plate A	wt%	0.15	0.52	1.32	0.2	0.01	0.21	0.016	0.57	0.19
	at.%	0.13	0.49	1.33	0.39	0.018	0.97	0.028	0.33	0.20
Plate B	wt%	0.17	0.64	1.39	0.21	0.013	0.23	0.013	0.50	–
	at.%	0.15	0.60	1.40	0.41	0.023	1.06	0.022	0.29	–
Forging	wt%	0.02	0.76	0.72	0.21	0.014	0.24	0.012	0.62	0.34
	at.%	0.017	0.72	0.72	0.41	0.025	1.11	0.021	0.36	0.36
Weld A	wt%	0.28	0.59	1.49	0.51	0.016	0.09	0.016	0.39	0.06
	at.%	0.24	0.56	1.5	1.01	0.03	0.42	0.03	0.23	0.06
Weld B	wt%	0.30	0.58	1.63	0.61	0.017	0.08	0.012	0.39	0.10
	at.%	0.26	0.55	1.64	1.20	0.03	0.37	0.021	0.22	0.10

Table 2
Thermal history of as-received (reference) and long-term thermally-aged commercial alloys

Material type	Heat No.	Heat treatment[a] (as-received)	Thermal ageing conditioning
Plate A	C5114-1	austenitized 899–927°C, WQ, tempered 649°C, AC, stress-relieved 593–621°C for 29 h, FC	93 000 h, Arkansas Unit-1, 280°C
Plate B HSST 02	A1195-1	austenitized 829–913°C for 4 h, WQ, tempered 649–677°C for 4 h,FC, stress-relieved 593–621°C for 40 h,FC	
Forging	ANK-191	austenitized 854–877°C for 4 h, WQ, tempered 666–688°C for 10 h, WQ, stress-relieved 593–621°C for 30 h, FC	103 000 h, Oconee Unit-3, 282°C
Weld A	WF-193	stress-relieved 593–621°C for 29 h, FC	93 000 h, Arkansas Unit-1, 280°C
Weld B	WF-209-1	stress-relieved 593–621°C for 30 h, FC	103 000 h, Oconee Unit-3, 282°C

[a]WQ = water quench, AC = air cool, FC = furnace cool.

power times when the surveillance material were removed. The heat treatment and stress relief history of these materials are given in Table 2.

3. Experimental

The technique of atom probe field ion microscopy (APFIM) is particularly well suited to the characterization of these pressure vessel steels because of its near atomic resolution and its ability to chemically analyze features on the near atomic scale [20]. The microstructural characterizations were performed in the ORNL energy-compensated atom probe field ion microscope [21].

The experimental conditions required to obtain accurate APFIM data are well known for these ferritic steels. In particular, it is necessary to cool the specimen to a temperature of 50 K to avoid a systematic error on the copper level measurement. Field ion specimens were electropolished using standard procedures [20] from blanks that were cut from Charpy specimens. All compositions reported in this work are quoted in atomic percent. The energy-compensated atom probe used in these investigations has a sufficient mass resolution ($m/\Delta m = \sim 2500$) to separate all isotopes. Also peak overlaps of species having the same mass-to-charge ratio were accounted for in composition determinations by standard methods [22]. The pile-up effect, known to occur in these steels, was correct with the method proposed by Menand et al. [23].

4. Results

A parallel set of experiments has been undertaken with unaged and thermally-aged materials. The results concerning the chemical compositions of the ferritic matrix are summarized in Table 3. Concentration uncertainties (2σ) due to counting statistics, as given by the standard deviation $\sigma = [X(1-X)/N]^{1/2}$, where X is the measured concentration of an element and N is the number of atoms collected in each analysis. It must be noted that these reactor pressure vessel steels can exhibit significant compositional variation from one specimen to another, particularly since only a small volume of material ($\approx 3 \times 10^{-25}$ m^3) is sampled from any given specimen. The values in Table 3 are an average of several experiments in which N

Table 3
Chemical compositions (at.%) of the ferritic matrix determined by APFIM in unaged (UnA) and long-term thermal-aged (Th-A) materials

	Plate A		Plate B		Forging		Weld A		Weld B	
	UnA	Th-A	UnA	Th-A	UnA	Th-A	UnA	Th-A	UnA	Th-A
Cu	0.11 ± 0.05	0.09 ± 0.03	0.09 ± 0.05	0.07 ± 0.03	0.03 ± 0.01	0.03 ± 0.02	0.14 ± 0.03	0.15 ± 0.05	0.16 ± 0.03	0.17 ± 0.02
Ni	0.64 ± 0.13	0.74 ± 0.10	0.74 ± 0.15	0.50 ± 0.11	0.72 ± 0.07	0.63 ± 0.10	0.45 ± 0.06	0.45 ± 0.09	0.42 ± 0.05	0.43 ± 0.05
Mn	0.95 ± 0.15	1.30 ± 0.13	0.64 ± 0.14	1.05 ± 0.17	0.48 ± 0.06	0.53 ± 0.09	1.20 ± 0.10	0.90 ± 0.12	1.24 ± 0.09	1.22 ± 0.09
Si	0.41 ± 0.10	0.62 ± 0.09	0.44 ± 0.12	0.43 ± 0.10	0.50 ± 0.06	0.44 ± 0.08	1.05 ± 0.10	0.80 ± 0.12	1.73 ± 0.10	1.49 ± 0.09
P	0.02 ± 0.02	0.003 ± 0.003	0.01 ± 0.01	0.007 ± 0.007	0.02 ± 0.01	0.003 ± 0.003	0.03 ± 0.03	0.02 ± 0.02	0.05 ± 0.02	0.07 ± 0.02
C	–	0.006 ± 0.006	0.02 ± 0.02	–	0.004 ± 0.004	–	0.005 ± 0.005	–	0.008 ± 0.008	0.03 ± 0.01
Mo	0.11 ± 0.05	0.17 ± 0.04	0.12 ± 0.06	0.15 ± 0.06	0.12 ± 0.03	0.08 ± 0.03	0.18 ± 0.04	0.14 ± 0.05	0.20 ± 0.04	0.23 ± 0.04
Cr	0.11 ± 0.05	0.06 ± 0.02	0.04 ± 0.04	0.08 ± 0.05	0.15 ± 0.03	0.20 ± 0.05	0.03 ± 0.03	0.03 ± 0.01	0.07 ± 0.02	0.06 ± 0.02

All compositions are the average of several experiments ($\pm 2\sigma$).

is typically ~60 000 atoms. The error bars quoted are based on counting statistics (i.e., the total number of atoms collected) and do not reflect the composition variations from one region to another. As copper repartitioning is a major contributing factor in the embrittlement of pressure vessel steels, particular attention has been paid to this element. The composition variation was particularly evident in the measurement of the copper level in the plates A and B. Severe fluctuations in the copper content from one specimen to another were observed, varying from 0.02 to 0.14 at.% Cu. In such cases, the error bars were also calculated based on the average compositions of different volumes. More realistic values are 0.10 ± 0.03 at.% Cu (plate A) and 0.06 ± 0.05 at.% Cu (plate B). However, the average copper solute concentration determined in the ferritic matrix is consistent with the nominal level for the two plates and the forging materials. In contrast, a depletion of copper was observed in the matrix of the weld A and weld B metals for both unaged and thermally-aged samples. This depletion cannot be due to the spatial fluctuation mentioned above since only 70% of the nominal level was detected.

A coarser microstructural characterization with the techniques of optical metallography and analytical transmission electron microscopy has been performed on the weld A material [24]. The low copper level in the carbides or in inclusions cannot fully account for the measured copper depletion from the nominal 0.25% Cu to the level of 0.17% Cu measured in the matrix.

The stress relief heat treatment for the weld A and weld B materials was performed at a temperature between 593 and 621°C. The predicted solubility limit of copper in the iron–copper binary system ranges between 0.17 and 0.24 at.% for these two temperatures. The detected value of 0.17 at.% can be simply explained by the solubility limit of copper in the ferritic solid solution at the stress relief treatment. This suggests the formation of other copper-rich precipitates during the stress-relief heat treatment, or also during the furnace cooling period (at a cooling rate of ~8°C/h to ~310°C), even though they have not been detected in this investigation. However, coarse copper-enriched precipitates have been detected at grain boundaries by atom probe field ion microscopy of A533B steels [7].

The Si and Ni contents of the matrix are, within the standard deviation, in good agreement with the nominal composition of the alloy. The depletion of carbon and molybdenum in the materials suggests the presence of a high volume fraction of carbides, particularly in the two plate (A and B) and forging materials. This high volume fraction of carbides in these materials may also explain the observed phosphorus matrix depletion. Indeed, phosphorus is often encountered at ferrite/carbide interfaces. In all materials, the detected level of manganese is always slightly lower than the nominal concentration. This depletion is due to its presence in cementite carbides, as shown below.

In order to characterize the structure of these unaged and long-term thermally-aged materials, analyses were performed on both the carbides and the matrix. The more common features encountered in the atom probe analyses of these steels are M_3C cementite carbides and molybdenum-containing carbides.

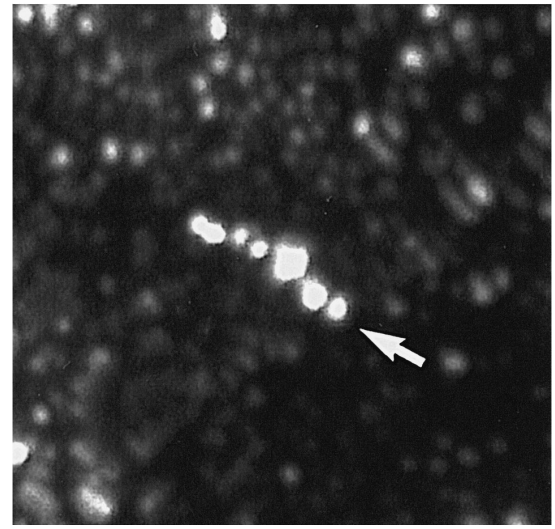

Fig. 1. Field ion micrograph of disk-shaped molybdenum carbides in the weld B surveillance material.

Molybdenum-containing carbides were frequently observed in both unaged and thermally-aged specimens. The small carbides have a disc, needle or spherical shape, whereas the larger precipitates are generally spherical, as shown in Figs. 1 and 2. The size of the observed carbides was determined to be between 5 to 20 nm. The Mo:C ratio, in both the unaged and thermally-aged materials, is close to that of Mo_2C.

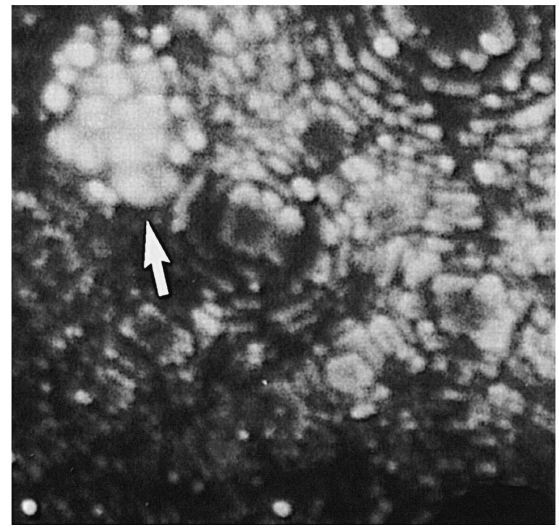

Fig. 2. Field ion micrograph of spherical molybdenum carbides in the weld B surveillance material.

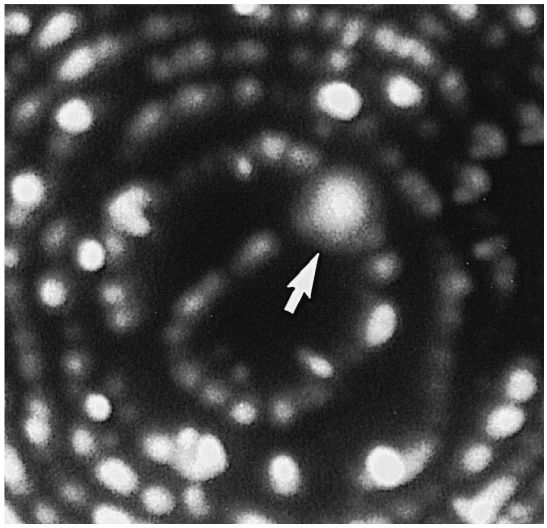

Fig. 3. Field ion micrograph of a decorated dislocation in the unaged forging material. Bright and diffuse spots are molybdenum or phosphorus.

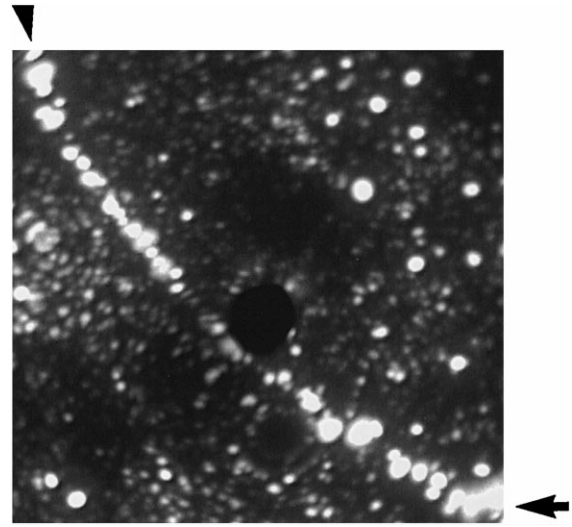

Fig. 5. Decorated grain boundary in the weld B long-term thermally-aged surveillance material. Bright spots are ultrafine Mo_2C carbides.

In addition, molybdenum atoms were also detected in the vicinity of dislocations, sometimes associated with carbon and phosphorus, as evident in Figs. 3 and 4. A field ion image of a dislocation having a Burgers vector component normal to the specimen surface is shown in Fig. 3. The presence of a dislocation converts the usual pattern of concentric rings at a crystallographic pole into a spiral at its point of emergence on the specimen surface [25]. Bright spots, characteristic of molybdenum atoms, which decorate the dislocation can be observed near its point of emergence. The sequence of evaporation of the atoms during the atom probe analysis of the core of the dislocation is shown in Fig. 4. The atoms on each line are representative of ~ 0.29 nm of material field evaporated from the speci-

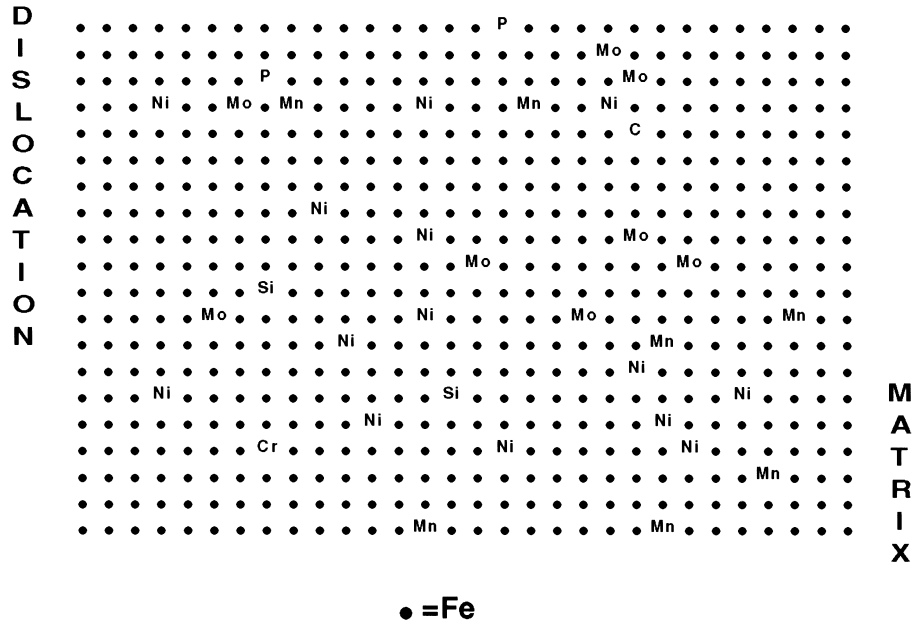

Fig. 4. Sequence of arrival of ions at the detector from the analyzed dislocation (see Fig. 3). Note the Mo, C and P enrichments in the core of the dislocation. Each line represents the removal of approximately 0.29 nm of material from the specimen.

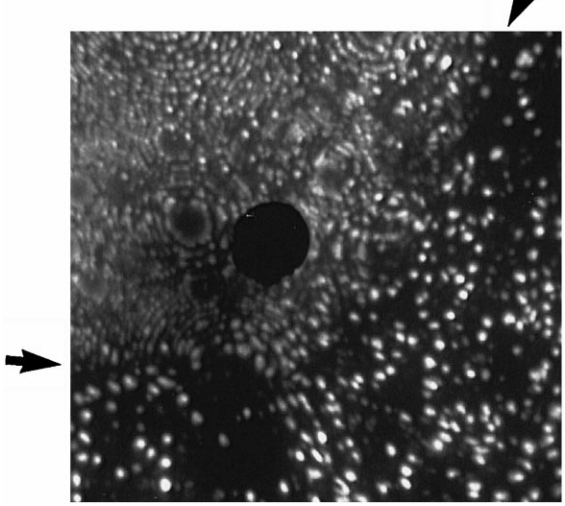

Fig. 6. Darkly-imaging cementite and brightly-imaging ferrite in long-term thermally-aged plate B material. Bright region at the interface is Mo_2C carbide (see Fig. 7).

men. This figure clearly indicates that Mo, P and C are detected in the vicinity of the dislocation. The concentrations of these elements decrease significantly in regions far removed from the dislocation.

In addition to the Mo_2C carbides and the cores of decorated dislocations, molybdenum is also observed at the grain boundaries. A field ion image of a grain boundary observed in the long-term thermally-aged weld B material is shown in Fig. 5. This micrograph clearly indicates that the grain boundary is decorated with a 1–2 nm thick layer of molybdenum carbides precipitates. This type of decoration has been observed in various Russian and Western steels and is a common feature of molybdenum-containing pressure vessel steels [7,8,26].

Another common feature encountered in these materials is M_3C cementite carbides. A field ion micrograph of a cementite–ferrite interface observed in the thermally-aged plate B material is shown in Fig. 6. The ferrite can be easily recognized by the presence of crystallographic poles (i.e., families of concentric rings), which are not evident in the darkly-imaging cementite phase. A brightly-imaging molybdenum carbide precipitate is also evident at the interface. A composition profile starting in this molybdenum carbide and emerging immediately into a cementite precipitate located at the interface is shown in Fig. 7. It is evident from this composition profile that there is a large Fe and Mn content in the cementite but little solubility of the Fe, Cr, and Mn alloying elements in the Mo_2C precipi-

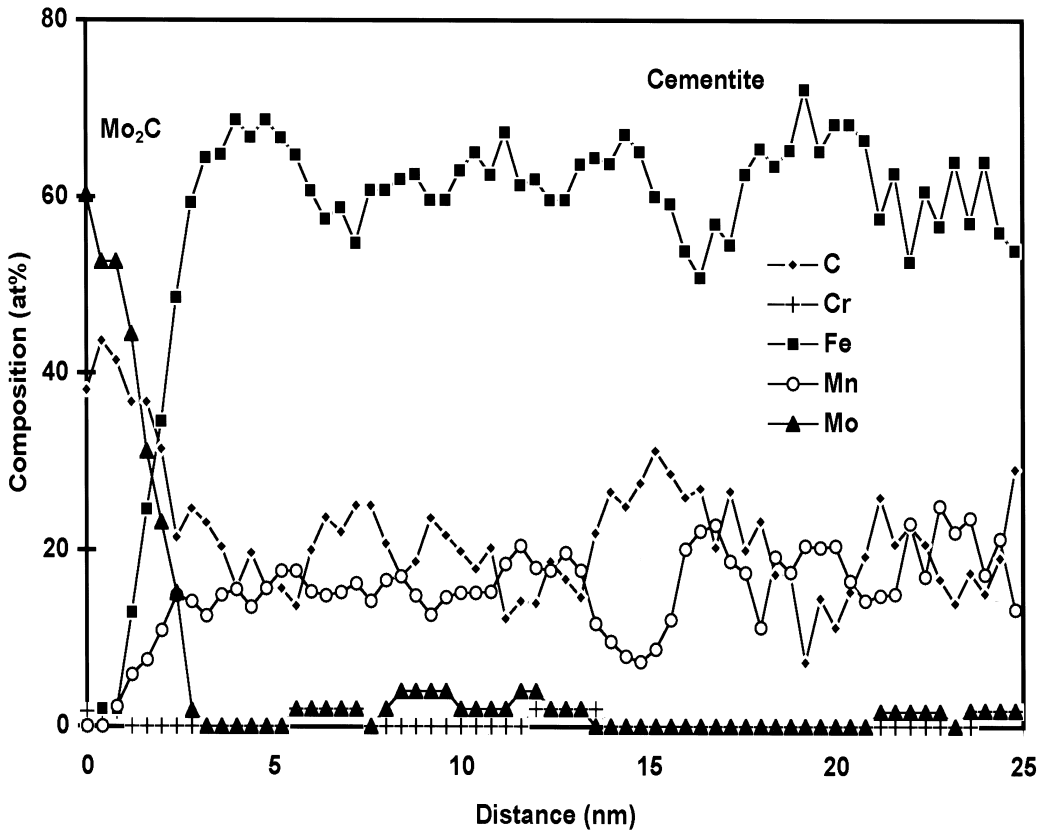

Fig. 7. Composition profile through a molybdenum carbide and cementite in long-term thermally-aged plate B surveillance material.

Table 4
Atom probe analyses of the cementite carbides. Comparison of the atom probe results with the Thermocalc™ predictions

	Fe	C	Mn	Mo	Cr	Ni
Plate A unaged, stress-relieved 593–621°C for 29 h, FC						
Thermocalc prediction: 620°C	59.1	25.0	11.1	1.5	3.1	0.1
Thermocalc prediction: 593°C	57.5	25.0	12.5	1.6	3.3	0.1
Atom probe experiment: 593–620°C	64 ± 0.8	25.6 ± 0.7	8.7 ± 0.5	1.2 ± 0.2	0.5 ± 0.1	–
Thermocalc prediction: 300°C	36.5	25.0	29.9	3.4	5.0	0.1
Plate B long-term thermally-aged, stress-relieved 593–621°C for 40 h, FC, 93 000 h at 280°C						
Thermocalc prediction: 620°C	61.8	25.0	11.6	1.5	–	0.1
Thermocalc prediction: 593°C	60.4	25.0	12.9	1.5	–	0.1
Thermocalc prediction: 300°C	42.1	25.0	29.3	3.35	–	0.2
Atom probe experiment: 93,000 h at 280°C	61.1 ± 0.1	25.4 ± 0.9	11.9 ± 0.7	0.9 ± 0.2	–	0.2 ± 0.1

tate. In order to determine if there was an effect of the ~ 10 years thermal aging treatment on the evolution of the composition of cementite, analyses were performed in unaged and thermally-aged specimens. Analyses were performed in plate A for the unaged specimen and in plate B for the thermally-aged one. The chemical compositions and stress-relief heat treatment of these two materials are so similar that they can be compared. In addition, the atom probe results were compared to thermodynamic predictions [27]. Thermocalc™ calculations were performed at two temperatures, 620 and 593°C, within the stress-relief heat treatment and also at 300°C, the temperature at which specimens were thermally-aged (93 000 h in the case of plate B). The results are summarized in Table 4.

The atom probe results revealed, in both unaged and thermally-aged materials, carbides with classic M_3C stoichiometry, where M stands for Fe and Mn (in majority), Mo, Cr and Ni (in minority) and also Cu and V (as traces, 0.02 at.%). These results are similar to those observed in previous analyses of the Chooz A pressure vessel steel [9] and weld metal [20]. In addition, the experimental compositions are in good agreement with the Thermocalc™ predictions for materials aged at 593–620°C. In all cases, the compositions are comparable to the predicted values at ~ 600°C. This agreement indicates that long-term thermal aging has no significant impact on the evolution of the microchemistry of cementite carbides.

These initial APFIM microstructural examinations performed on unaged and long-term, low temperature, thermally-aged materials show no significant evolution of the structure of the material. No phase transformation has been observed for this low temperature heat treatment. Unaged materials and materials thermally-aged for approximately 10 years have a similar ferritic matrix chemistry and carbide compositions. These results are consistent with the observed mechanical properties of these materials [17]. A general review of the data on thermal-aged material indicates virtually no significant change in the impact data. Only small variations in the Charpy V-notch impact properties were observed for all materials after exposure at the thermal-aging temperature. Small increases (~ 1°C) in transition temperature were observed for the forging metal and weld B surveillance materials aged at 103,000 h, and their upper-shelf energies demonstrated small decreases (3 to 11 J). The Charpy V-notch results for plate A and weld metal A aged for 93 000 h revealed differences in that the 41 J transition temperatures for both materials decreased slightly.

Also, and especially for the weld materials, the copper remains in solid solution with a concentration following the solubility of copper in iron for unaged specimens. A metastable solid solution is observed for thermally-aged specimens. This confirms that the thermal mobility of copper in iron at 300°C is effectively zero.

5. Conclusion

Microstructural characterization of long-term (~ 100 000 h) thermally-aged (300°C) and unaged surveillance materials obtained from the B and W Owners Group was performed. Two welds, two plates and one forging material were investigated. The comparison between the thermally-aged materials and unaged materials permitted, for the first time, the investigation of a potential thermal aging effect. Although a general review of the thermal-aging data indicates that there may be some propensity toward embrittlement in sensitive materials [11,12], the materials examined in this study did not exhibit any significant embrittlement or microstructural evolution. The same matrix copper level was found before and after the long thermal aging treatment. In the two welds, a significant decrease of the copper level in the matrix over the nominal bulk composition was found and may be due to copper precipitation during the stress-relief heat treatment. This APFIM comparison of the microstructures in all three conditions is consistent with the measured mechanical properties (transition temperature shift), i.e., no significant changes in either the microstructure or the mechanical properties has been observed.

Acknowledgements

The materials for this study were provided by the B&W Owners Group. The authors would like to thank M.J. De Van and W.A. Pavinich of B&W Nuclear Technologies for their assistance. This research was sponsored by the Division of Materials Sciences, US Department of Energy, under contract DE-AC05-96OR22464 with Lockheed Martin Energy Research Corp. and by the Office of Nuclear Regulatory Research, US Nuclear Regulatory Commission under inter-agency agreement DOE 1886-8109-8L with the US Department of Energy. This research was conducted utilizing the Shared Research Equipment (SHaRE) User Program facilities at Oak Ridge National Laboratory.

References

[1] M.K. Miller, S.S. Brenner, Res. Mechan. 10 (1984) 161.
[2] M.K. Miller, J.A. Spitznagel, S.S. Brenner, M.G. Burke, in: Proc. 2nd Int. Symp. on Environmental Degradation of Materials in Nuclear Power Systems – Water Reactors, Monterey, CA, 1985, eds. J.T.A. Roberts, J.R. Weeks and G.J. Theus (American Nuclear Society, La Grange Park, IL, 1986) p. 523.
[3] M.G. Burke, S.S. Brenner, J. Phys. (Paris) 47 (C2) (1986) 239.
[4] S.P. Grant, S.L. Earp, S.S. Brenner, M.G. Burke, in: Proc. 2nd Int. Symp. on Environmental Degradation of Materials in Nuclear Power Systems – Water Reactors, Monterey, CA, 1985, eds. J.T.A. Roberts, J.R. Weeks and G.J. Theus (American Nuclear Society, La Grange Park, IL, 1986) p. 385.
[5] M.K. Miller, M.G. Burke, J. Phys. (Paris) 48 (C6) (1987) 429.
[6] M.G. Burke, M.K. Miller, J. Phys. (Paris) 49 (C6) (1988) 283.
[7] M.K. Miller, M.G. Hetherington, M.G. Burke, Metall. Trans. 20A (1989) 2651.
[8] M.K. Miller, M.G. Burke, J. Nucl. Mater. 195 (1992) 68.
[9] P. Pareige, J.C. Van Duysen, P. Auger, Appl. Surf. Sci. 67 (1993) 342.
[10] P. Pareige, M.K. Miller, Appl. Surf. Sci. 67 (1996) 370.
[11] M.K. Miller, D.T. Hoelzer, F. Ebrahimi, J.R. Hawthorne, M.G. Burke, J. Phys. (Paris) 48 (C6) (1987) 423.
[12] M.K. Miller, D.T. Hoelzer, F. Ebrahimi, J.R. Hawthorne, M.G. Burke, in: Proc. 3rd Int. Symp. on the Environmental Degradation of Materials in Nuclear Power Systems – Water Reactors, Sept 1987, Traverse City, MI, eds. G.J. Theus and J.R. Weeks (The Metallurgical Society, Pittsburgh, PA, 1988) p. 133.
[13] S.L. Hoyt et al., Trans. ASME 68 (1946) 571.
[14] R.K. Nanstad, D.J. Alexander, W.R. Corwin, E.D. Eason, G.R. Odette, R.E. Stoller, J.A. Wang, Preliminary review of data regarding chemical composition and thermal embrittlement of reactor vessel steels, ORNL/NRC/LTR–95/1, Oak Ridge National Laboratory, Jan. 1995.
[15] A.W. Pense, R.D. Stout, E.H. Kottcamp, Welding J. 42 (1963) 5415.
[16] C.Z. Serpan, H.E. Watson, Nucl. Eng. Des. 11 (1970) 393.
[17] C.Z. Serpan, H.E. Watson, J.R. Hawthorne, Nucl. Eng. Des. 11 (1970) 368.
[18] M.J. Lowe, Jr., in: Radiation Embrittlement and Surveillance of Nuclear Reactor Pressure Vessels: An International Study, ASTM STP 819, ed. L.E. Steele (American Society for Testing and Materials, Philadephia, PA, 1983) p. 146.
[19] M.J. De Van, A.L. Lowe, Jr., S. Wade, in: Effects of Radiation on Materials: 16th Int. Symp., ASTM STP 1175, eds. A.S. Kumar, D.S. Gelles, R.K. Nanstad and E.A. Little (American Society for Testing and Materials, Philadelphia, PA, 1993) p. 268.
[20] M.K. Miller, G.D.W. Smith, Atom Probe Microanalysis: Principles and Applications to Materials Problems (Materials Research Society, Pittsburgh, PA, 1989).
[21] M.K. Miller, J. Phys. (Paris) 47 (C2) (1986) 493.
[22] M.K. Miller, A. Cerezo, M.G. Hetherington, G.D.W. Smith, Atom Probe Field Ion Microscopy (Oxford University, Oxford, 1996).
[23] A. Menand, T. Al-Kassab, S. Chambreland, J.M. Sarrau, J. Phys. (Paris) 49 (C6) (1988) 353.
[24] K.R. Lawless, A.L. Lowe Jr., in: Effects of Radiation on Materials: 15th International Symposium, ASTM STP 1125, eds. R.E. Stoller, A.S. Kumar and D.S. Gelles (American Society for Testing and Materials, Philadelphia, PA, 1992) p. 186.
[25] K.M. Bowkett, D.A. Smith, Field Ion Microscopy (North-Holland, Amsterdam, 1970).
[26] M.K. Miller, R. Jayaram, K.F. Russell, J. Nucl. Mater. 225 (1995) 215.
[27] B. Sundman, B. Jansson, J.-O. Anderson, CALPHAD: Comput. Coupling Phase Diagrams Thermochem. 9 (1985) 153.